RSC Advances

PAPER

View Article Online
View Journal | View Issue

Cite this: *RSC Adv.*, 2016, **6**, 8006

Indiene 2D monolayer: a new nanoelectronic material

Deobrat Singh,[a] Sanjeev K. Gupta,*[b] Igor Lukačević*[c] and Yogesh Sonvane[a]

One atom thick monolayer nanostructures consisting of group III, IV and V elements are drawing ever more attention for their extraordinary electronic properties. Through first principles calculations, we systematically investigate structural and electronic properties of the corresponding indium monolayers in three different allotropic forms: planar, puckered and buckled. Our study shows that the planar and buckled allotropes are stable and show metallic and semiconducting behavior, respectively. Their stability and electronic properties cannot be easily correlated to those of similar elemental monolayer structures. The van Hove singularity is observed in the electronic density of states which could lead to an increase in the electronic conductivity, opening paths to new electronic applications. Strain engineering is applied in order to determine the changes in the electronic behavior and band gap properties. The planar allotrope remains metallic under both compressive and tensile strain, while the buckled allotrope changes from an indirect semiconductor to a metal. Our study demonstrates that the indiene nanostructures possess diverse electronic properties, tunable by strain engineering, which have potential applications in nanoelectronics and for nanodevices.

Received 3rd December 2015
Accepted 30th December 2015

DOI: 10.1039/c5ra25773e

www.rsc.org/advances

1 Introduction

Since the discovery of graphene[1–3] other two-dimensional (2D) group-III, IV and V nanostructures have attracted a lot of interest from physicists, chemists, and materials scientists.[4–6] One of the trends in today's materials science is predicting two-dimensional materials, consisting of only one or two elements, which are possible candidates for a wide range of applications: from electronic devices, like field effect transistors (FET) or bipolar junction transistors (BJT), through optoelectronic devices, like light emitting diodes (LED) or solar cells, to nanomaterials. The most important feature of these novel materials is that they possess an intrinsic band gap, contrary to graphene which suffers from its absence and, thus, has limited practical applications. This band gap is usually indirect, but it has been shown that it can be easily modified and converted to a direct band gap or even closed using strain or an external electric field. Further tuning can be obtained by changing the number of layers or the stacking order of the layers.

Recently, arsenene and antimonene, which are single-atom-thick layers of arsenic and antimony, have been proposed as new members of group-V monolayer nanostructures.[7–11] These arsenic[8,12] and antimony[13] nanosheets have a buckled or a puckered structure, similar to those of blue or black phosphorene, respectively.[14–16] Their buckled and puckered allotropes behave as indirect semiconductors with band gaps in the range between 0.3 and 1.6 eV. An indirect to direct band gap transition, or its closing, have been proposed under the influence of strain, contrary to the case of phosphorene, where a direct to indirect band gap transition has been proposed.[14] Previously considered group-IV single-element monolayer structures (apart from carbon's graphene) refer to Si (silicene), Ge (germanene) or Sn (tinene) atoms.[17,18] They exhibit buckled monolayer structures due to the hybridization of sp^2 and sp^3 orbitals. Much progress has been done in the case of these materials as they have already been experimentally verified, although only on substrates and not as the stand-alone materials.[19–21] They have a much larger band gap than graphene, due to their low-buckled geometry and larger atomic intrinsic spin–orbit coupling strength, in the range of up to 0.1 eV, which is on the other hand much smaller than in the case of group-V monolayer materials. However, they draw attention as Dirac materials with quantum spin Hall effect and a band gap which is easily tunable using an external electric field[22] or by doping.[23] Up to now, out of the group-III elements, only aluminium has been used to predict a monolayered material – aluminene.[24] Aluminene has only one stable allotrope with a planar structure. It behaves as a metal with specific features in the electronic density of states which could point to the occurrence of chiral superconductivity. Monolayer materials consisting of other group-III elements are only mentioned in the literature as

[a]*Department of Applied Physics, S. V. National Institute of Technology, 395007 Surat, India*

[b]*Department of Physics and Electronics, St. Xavier's College, 380009 Ahmedabad, India. E-mail: sanjeev.gupta@sxca.edu.in*

[c]*Department of Physics, University J. J. Strossmayer, 31000 Osijek, Croatia. E-mail: ilukacevic@fizika.unios.hr; Fax: +385 31232701; Tel: +385 31232713*

unstable in any allotropic structure considered so far, but arguments against this have not yet been published.

In this paper we study monolayered materials made of indium atoms, named indiene in analogy with previously reported similar materials. Indium is considered because: (1) it is a soft, silvery metal that is stable in air and water; (2) it is widely applied as a low melting point metal alloy in industrial applications; (3) it is used in the production of transparent conductive coatings of indium tin oxide (ITO) on glass, an important part of the photoelectronic industry; (4) indium nitride, phosphide and antimonide are semiconductors used in transistors and microchips, the basics of electronic applications; (5) it is used as a coating for bearings in high-performance aircraft engines, fusible alloys and in solders. All these applications bring forth indium as a suitable candidate for a graphene-like monolayer material. But what kind of structures are energetically and dynamically stable in indiene? Does the indiene nanosheet have different electronic band structure features from the other known 2D nanosheets? Can it have high carrier mobility akin to graphene? To address these questions, we perform a first-principle theoretical investigation of the structural and electronic properties of indiene nanosheets in three different structures: planar, puckered and buckled.

Experimentally very large strains (up to 30%) can be applied to 2D layers.[25–27] These experimental studies confirm that strain engineering can be a very practical and useful path to modulate the electronic properties of 2D materials. Thus, we further focus on the effect of strain on the electronic band structures of stable indiene allotropes and its influence on the band gaps along with specific features exhibited by the electronic densities of states.

2 Computational details

We use first principles calculations based on fully self-consistent density functional theory (DFT),[28,29] which were carried out using the QUANTUM ESPRESSO package.[30] The generalized gradient approximation (GGA) in the form of the Perdew–Burke–Ernzerhof (PBE) exchange–correlation potential[31] has been applied. We use the norm conserving pseudopotential for an In atom with scalar-relativistic effects as available on the QUANTUM ESPRESSO web page. All three structures of indiene are periodic in the *xy*-plane and a vacuum space of 18 Å was applied in the *z*-direction to restrict the interaction between two adjacent planes introduced by Born–von Karman periodic conditions in the supercell approach employed during the construction of monolayers. Electron wavefunctions were expanded in the plane wave basis sets. The kinetic energy cutoff used for the plane wave basis sets is: 30 Ry, 45 Ry and 45 Ry, for planar, buckled and puckered structures, respectively. These basis sets gave us the total energies converged up to: 3.5×10^{-7} Ry, 1.5×10^{-4} Ry and 4.6×10^{-5} Ry, for planar, buckled and puckered allotropes, respectively. We approximate the Brillouin zone integration in reciprocal space using discrete Monkhorst–Pack meshes with $31 \times 31 \times 1$ *k*-points for planar and buckled, and $37 \times 37 \times 1$ *k*-points for the puckered system. We use 10^{-10} Ry in the self-consistent field calculation for the convergence of the total energy. The forces on each atom are converged below 0.01 eV $Å^{-1}$ during the structural optimization of both unit cell dimensions and atomic internal coordinates. All geometric structures were plotted using XCRYSDEN software.[32] Lattice dynamics calculations (the phonon spectrum, the density of states) are performed within the framework of the self-consistent density functional perturbation theory (DFPT). We use the same cutoff energies as in the total energy calculations, which are sufficient to keep the errors in vibrational frequencies below 5 cm^{-1}. In order to understand the detailed features of the phonon spectra, force constants are obtained on a $5 \times 5 \times 1$ *q*-point mesh. The dynamical matrices at arbitrary wave vectors are obtained using Fourier transform based interpolations.

3 Results and discussion

3.1 Structural properties and stability of indiene

First we present the results of the structural optimization of all three indiene structures: planar, buckled and puckered, and their relative stability concerning their total energies and lattice dynamics. The structure of the planar allotrope is like graphene's honeycomb structure, while the buckled and puckered allotropes are constructed in analogy with similar structures formed by elements like arsenic, phosphorous, silicon or germanium. The flat structure of graphene in the two-dimensional honeycomb structure has pure sp^2 hybridization. In all studied structures, each indium atom is bonded with three other indium atoms. The optimized geometric structures are shown in Fig. 1. After optimization, the relaxed lattice constants are $a = 4.25$ Å, $b = 5.68$ Å for the puckered structure, $a = 4.96$ Å for the planar structure and $a = 4.24$ Å for the buckled structure (Table 1). A comparison with similar monolayer structures of neighbouring elements shows that they follow the same trends as their bulk counterparts. Tin has the largest bulk lattice constant of 5.82 Å, and its buckled form, tinene,[18] has a larger unit cell than buckled indiene. Similarly, bulk indium has a larger lattice constant (4.59 Å) than bulk aluminum (4.05 Å), and so does its monolayer form, planar indiene, compared to planar aluminene.[24] The calculated puckering angle for the puckered allotrope of indiene is 101.71°, which lies between arsenene's 100.80° and phosphorene's 104.25°. Another angle in the puckered structure is 93.80°, which is slightly lesser in value than arsenene's 94.64°. In our case the calculated buckling height and angle are 1.54 Å and 94.51°, respectively. This angle is slightly larger than that of arsenene's 92.22°. Structural parameters of indiene and other similar materials for comparison are presented in Table 1.

Next we study the stability of all three structures of indiene. The calculated ground state total energies are −53.73, −53.66 and −53.69 eV per atom for the puckered, planar and buckled allotropes, respectively. In all these cases the ground state energies of indiene are nearly equal (Fig. 2). This means that from the total energy point of view, all three structures could be stable.

To confirm the stability of the studied structures we further regard the lattice dynamical stability of indiene monolayer

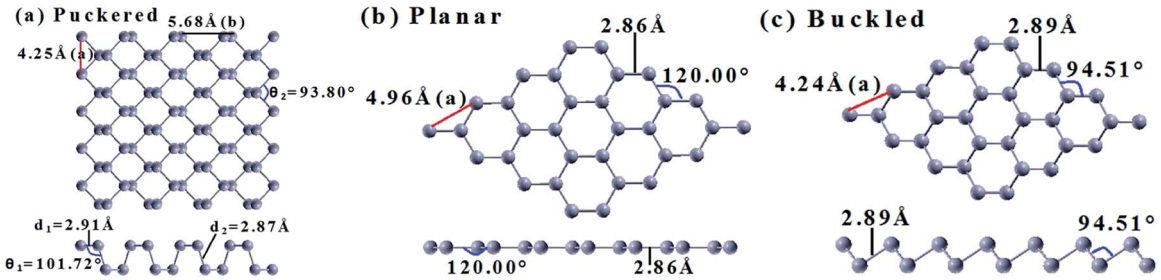

Fig. 1 Optimized geometries of (a) puckered, (b) planar and (c) buckled indiene. The red lines indicate the equilibrium lattice constants.

allotropes by calculating their full phonon dispersion curves. As seen in Fig. 3, planar and buckled structures of indiene have all real phonon frequencies. The puckered structure, on the other hand, shows imaginary frequencies for acoustic and some optic phonon modes throughout the whole Brillouin zone, similar to the aluminene case.[24] Thus, the puckered structure is not a lattice dynamically stable allotrope of indiene and for that reason our simulations indicate that it is not possible to obtain it using one of the above mentioned experimental techniques. Generally speaking, the stability of different allotropes of 2D graphite-like monolayer structures is very sensitive with respect to the electronic structure of the element in hand. For example, tinene is unstable in its planar allotrope. Cai *et al.*[18] stressed the importance of buckling in stabilizing the planar allotrope. However, this is not the case for indiene, consisting of indium atoms which have only one electron less than tin in the fifth electronic shell. Even more remarkably, it is completely opposite for aluminene,[24] having an isoelectronic structure with indium, with stable planar and unstable buckled allotropes. The lattice dynamical stability of other elements varies diversely, suggesting also the role of electron–phonon coupling, similar to the one played in graphene.[33,34] Phonon dispersion curves of buckled indiene resemble those of buckled tinene and antimonene, with separated acoustic and optic branches. Optic phonon modes are, however, less dispersed. The planar indiene allotrope contrasts that of aluminene in the optic mode which is separated from other optic modes, while in aluminene it approaches them at the *K* point of the Brillouin zone. Since indiene in the puckered configuration is not stable, as observed from its phonon spectra, we do not consider it for further analysis.

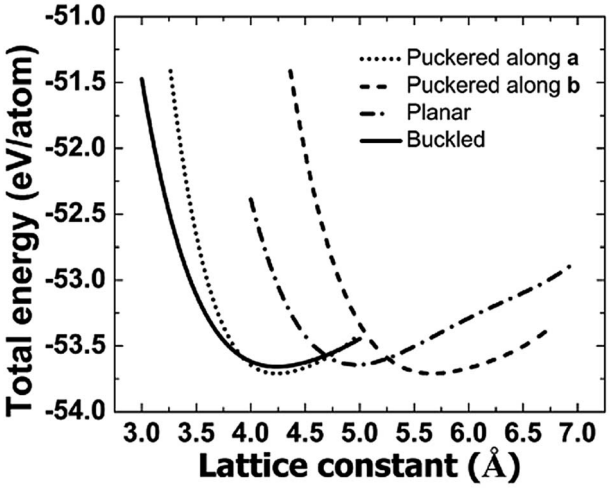

Fig. 2 Total energy of indiene allotropes as a function of lattice constants.

Graphene is manufactured by exfoliating graphite. Recently, phosphorene has also been manufactured by exfoliating black phosphorus,[35–37] similar to the case of graphene.[38] Bulk indium

Table 1 Structural parameters of indiene allotropes compared to similar materials: aluminene,[24] tinene,[18] arsenene,[8] antimonene[13] and phosphorene[14]

Allotr.	Elem.	E_{coh} (eV per atom)	Latt. const. (Å)		Bond leng. (Å)	Bond ang. (deg)
			a	*b*		
Planar	In	−1.81	4.96	—	2.86	120
	Al	−1.96	4.49	—	2.59	120
	As	−2.39	4.37	—	2.52	120
Buckled	In	−1.83	4.24	—	2.89	94.51
	Sn	—	4.52	—	2.70	113.50
	As	−2.99	3.61	—	2.50	92.22
	Sb	−4.57	4.01	—	2.84	89.90
Puckered	In	−1.88	4.25	5.68	2.91, 2.87	101.71, 93.80
	As	−2.95	3.68	4.77	2.50, 2.49	100.80, 94.64
	Sb	−4.63	4.48	4.31	2.91, 2.83	102.50, 95.00
	P	—	4.63	3.29	2.25, 2.22	104.25, 95.89

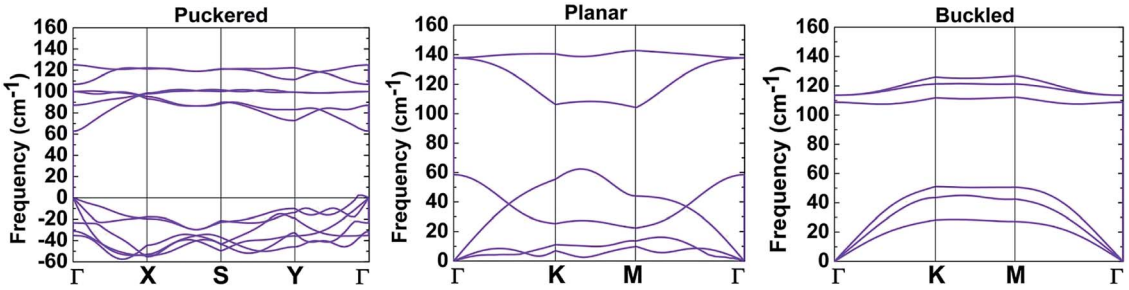

Fig. 3 Full phonon dispersion curves of puckered, planar and buckled allotropes of indiene.

has a body centered tetragonal unit cell (*I*4/*mmm*). It can be viewed as two planes of the same atoms, shifted by 1/4 of the unit cell length (in each direction, respectively) with respect to each other. If separated from the bulk, each pair of these two planes has exactly the same structure as the buckled monolayer of indium atoms. Thus, it may be possible to obtain the buckled indiene by exfoliating indium. Since the ground state total energies of both planar and buckled indiene are very close to

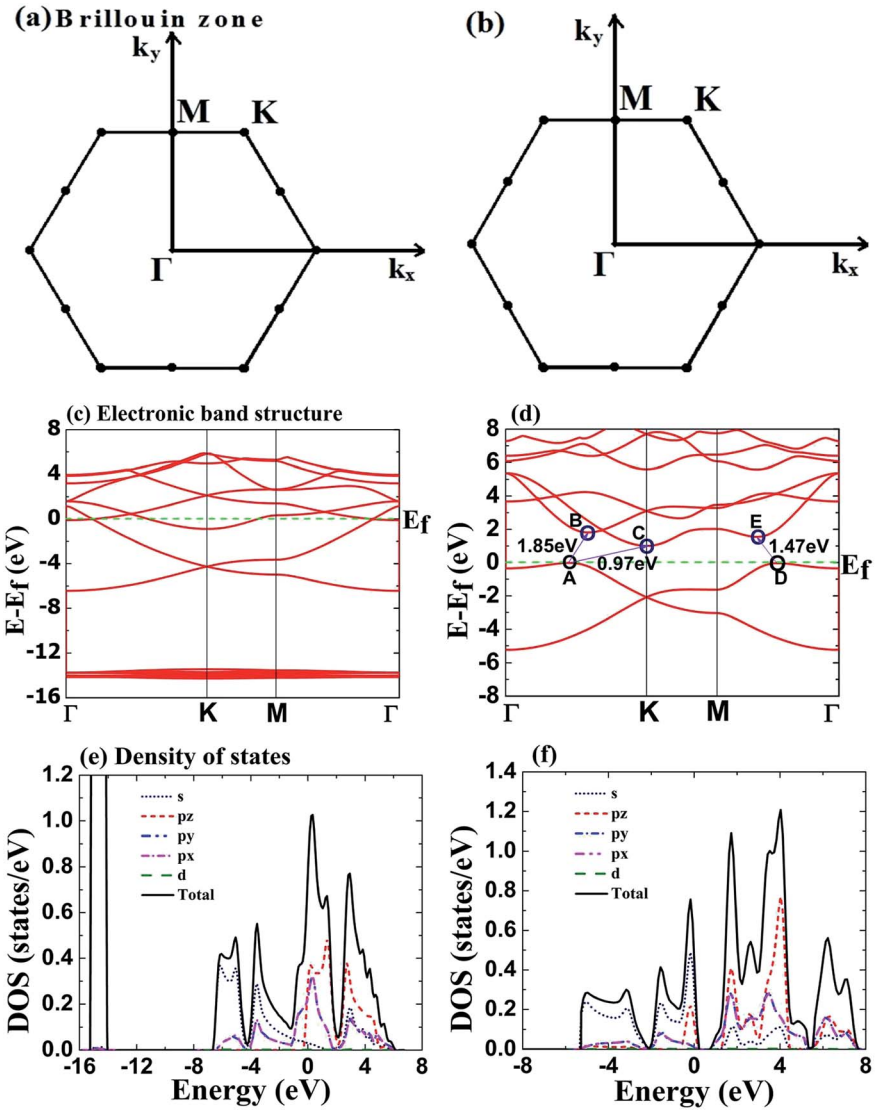

Fig. 4 Electronic properties of stable indiene allotropes. The hexagonal Brillouin zones of (a) planar and (b) buckled allotropes with high symmetry *k*-points. The electronic band structures of (c) planar and (d) buckled indiene with the Fermi level set to zero. Total DOS and partial DOS of (e) planar and (f) buckled indiene.

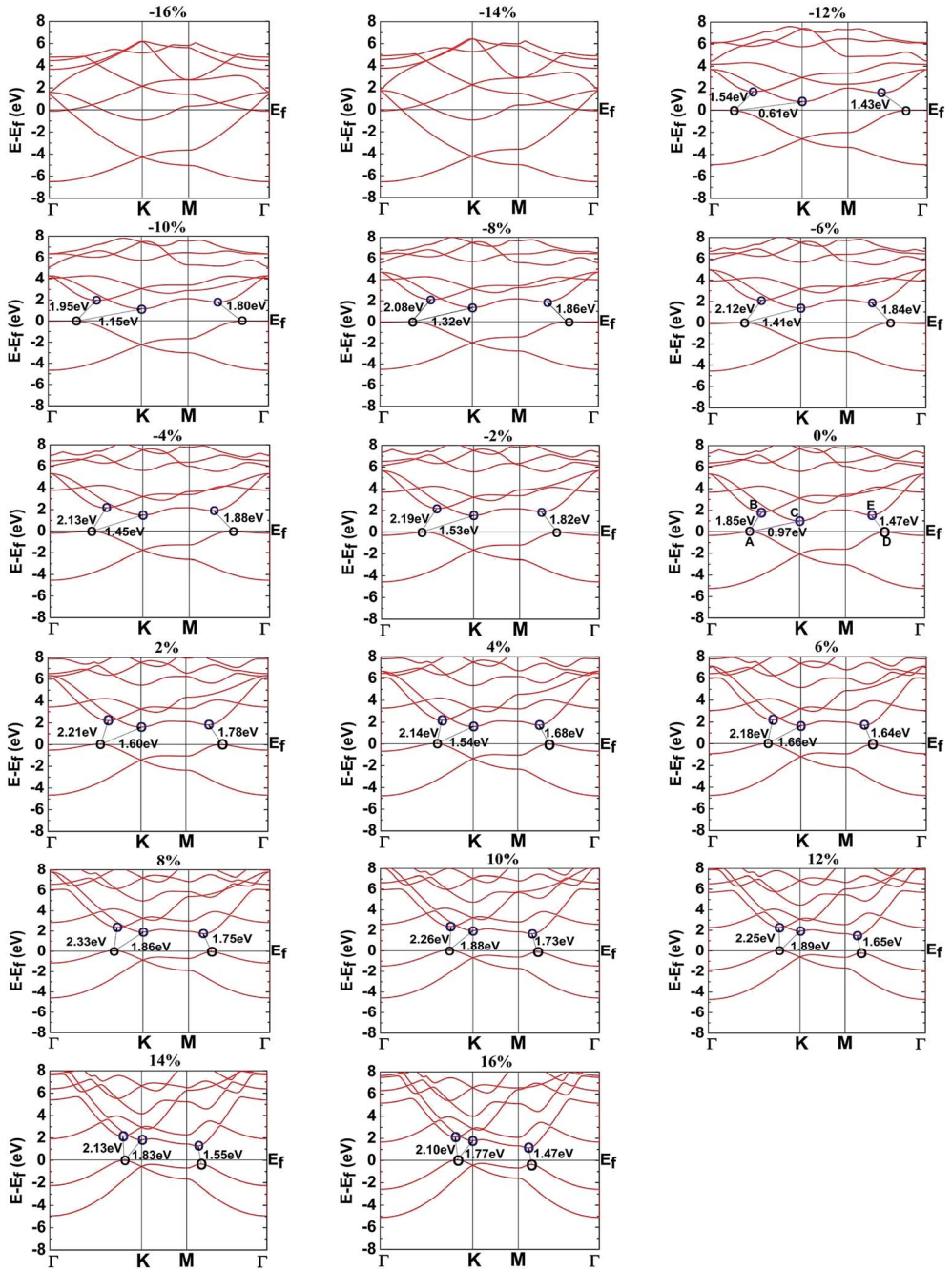

Fig. 5 The variation of electronic band structure with strain in buckled indiene.

that of the bulk indium, the possibility of manufacturing those indiene allotropes experimentally also exists. Our theoretical research brings motivation for experimental researchers to grow indiene.

3.2 Band structure

The electronic band structures, density of states (DOS) and partial density of states (PDOS), for the two stable structures (planar and buckled) with the equilibrium lattice constants, have been calculated. Electronic band structures together with the DOS and PDOS of individual orbitals of electronic states are shown in Fig. 4. The planar form behaves like a metal due to partial occupancies of hybrid sp^2 orbitals (σ and π). Two Dirac cones appear at the K point, at around 1.5 and -4.9 eV. The former one belongs to π bonds consisting primarily of p_z orbitals, while the latter one belongs to σ bonds having contributions from s and somewhat less from p_x and p_y orbitals. Two σ bands cross the Fermi level. The higher energy one belongs to p orbitals, while the lower energy one belongs to s, p and d orbitals. Dominance of p orbitals around the Fermi level is a common characteristic of 2D monolayer compounds, formed by sp^2 hybrid bonds, like silicene and phosphorene.[19,39]

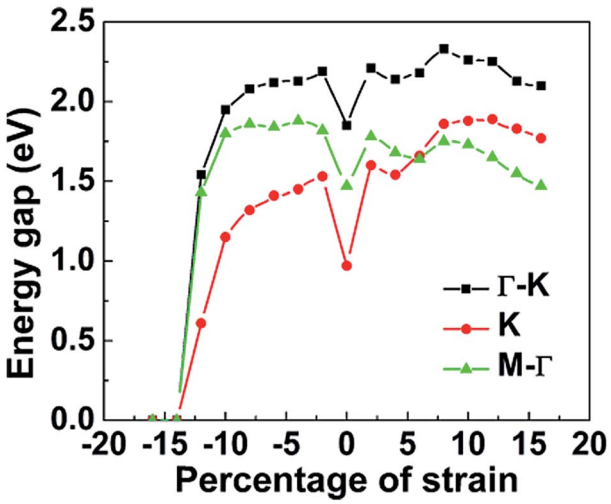

Fig. 6 Effect of strain on the band gap of buckled indiene. Electronic properties are governed by the features at *K* point, where the band gap closes for large tensile strains.

From an application point of view, a remarkable feature can be observed in electronic DOS (Fig. 4(e)). A van Hove singularity of the p orbital is found at an energy of about −0.2 eV, very close to the Fermi level. If one could shift the Fermi level so that it coincides with the van Hove singularity, one would obtain very large electrical conductivity with the application of gate voltage.[40]

On the other hand, the buckled form behaves like an indirect semiconductor, as small gaps appear as seen in Fig. 4(d). If one looks in the direction from Γ to K point, there are two energy gaps illustrated using points A (valence band maximum), B and C (conduction band minimum). The gap between the points A and B is 1.85 eV and between A and C it is 0.97 eV. In the direction from M to Γ point there is one energy gap between the points D and E, which is 1.47 eV. The energies of these bands, *i.e.* the positions of the above defined points are critical for the semiconducting character of buckled indiene. The valence band maximum (VBM) shows a character of almost pure s states close to −3 eV (Fig. 4(f)). The conduction band minimum (CBM) has a hybrid character from dominant p states and non-negligible contributions from s and d states.

In the next subsection we will discuss the effect of strain on the electronic band structures of planar and buckled indiene. This will allow us to see the changes in the energy gaps and consequently the changes in the electronic behavior of indiene.

3.3 Band gap strain engineering

We modify the band structures and their properties by the application of mechanical strain. Applying mechanical strain on a 2D structure is an easy and convenient method for modulating its electronic properties. Up to now, there are several theoretical studies which investigated the effect of strain on the electronic properties of monolayer structures.[8,13,14,41] Experimentally, it is known that one can induce spontaneous strain by depositing material layers on flexible substrates or by

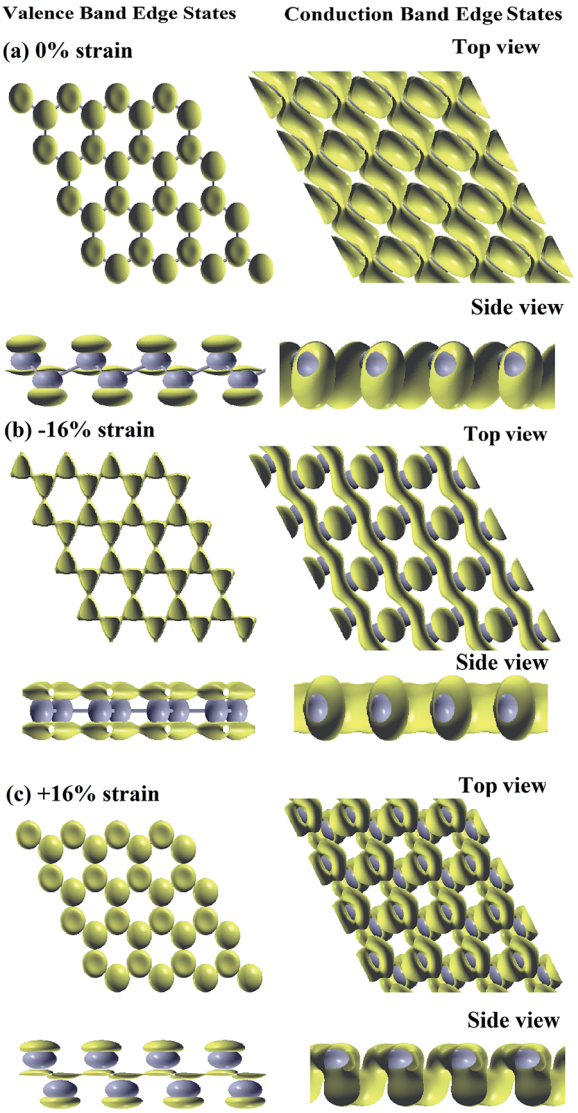

Fig. 7 The valence and conduction band charge densities of buckled indiene without strain, −16% and +16% strain in (a), (b) and (c), respectively, with top and side views of the 4 × 4 supercell.

using beam-bending apparatus[42] or scanning tunneling microscope tips for tensile strain.[43] In our theoretical study, strain was simulated by fixing and relaxing the respective lattice constants and the atomic internal coordinates of indiene allotropes.

3.3.1 Buckled indiene. We have performed a study on the effect of strain on the electronic properties of buckled indiene. In this case we apply negative and positive strains symmetrically along its lattice vectors (biaxial strain), because buckled monolayer structures show isotropic mechanical properties.[13] Strain is taken in steps of 2% between −16% and +16% from the unstrained geometry. This segment of strains proved to be sufficient to indicate significant changes. All these changes can be attributed to the shifts in the near gap states. Induced strain causes the atomic distances to change. As atoms in the 2D monolayer get closer or further away from each other, the overlaps of electron orbitals become larger or smaller. Different

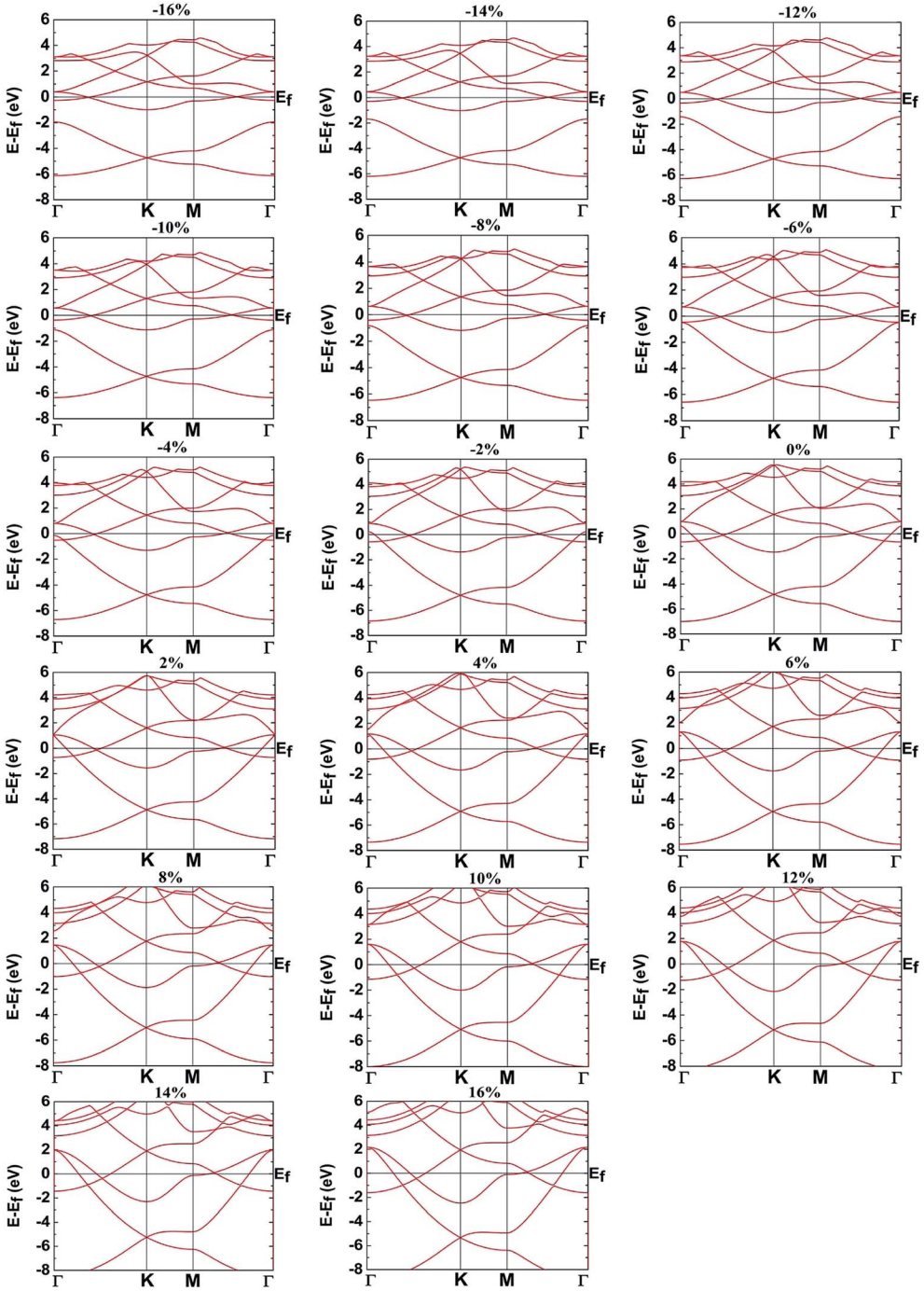

Fig. 8 The variation of electronic band structure with strain in planar indiene.

overlaps cause different superpositions of these orbitals, which results in the shifts of the electron energy states. After applying the compressive and tensile strain on the optimized geometric structure, the variation of the total energy of the system shows a parabolic form (Fig. 2). This confirms the energetic stability of the strained buckled indiene allotrope. The total energy of the system is more dominant in the case of positive and less dominant in the case of negative strain.

The changes in the electronic band structure under strain are shown in Fig. 5. When we apply negative strain, the energy gap initially increases, but then starts to continuously decrease along the Γ–K and M–Γ directions as well as at the K point, and buckled indiene retains its indirect semiconductor behavior until a −14% strain is applied. Beyond this strain the band gap quickly closes at all relevant points in the band structure and buckled indiene becomes metallic. This abrupt decrease of the band gap is attributed to the phase transition during which the

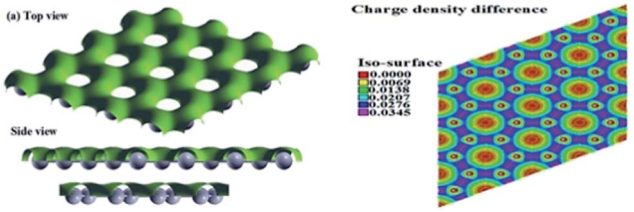

Fig. 9 Valence charge density distribution (a) of planar indiene with top and side views of the 4 × 4 supercell. Contour lines represent the charge density differences between the total and atomic densities from 0.00 to 0.0345 e Å^{-2}.

buckled allotrope is stretched into the planar one. These kinds of transitions were already found in some monolayer materials like pentagonal B_2.[44] In light of this, a 16% strain can be thought of as a critical strain at which the material changes its electronic behavior, *i.e.* it undergoes a semiconductor to semimetal transition. This transition possibly presents a very interesting application for engineering the electronic properties of buckled indiene. On the other side, after the initial increase, the energy gap continuously decreases between the relevant points when we apply a positive strain, but retains its semiconducting character even under large strains. The strain dependence of the band gap is shown in Fig. 6. In the compressive strain region there is some similarity with the band gap changes in buckled arsenene, as both cease to be semiconducting. The difference is that buckled arsenene becomes a semimetal at a −10% strain. In the tensile strain region the behavior is essentially different from the buckled arsenene[8] or antimonene,[13] which both turn metallic, while indiene remains a semiconductor. It might be interesting to note that there are no significant shifts of VBM and CBM points inside the Brillouin zone, as found in some similar materials, like arsenene.[8] The only shift is found at point B, which shifts to the left and seems to be aligning itself with point A at strains larger than +10%, thus exhibiting a direct gap between VBM and CBM. However, its importance is impaired by the more significant features between points A and C as indicated above.

We would also like to compare the amount of change in the band gap between the presently studied indiene and previously studied arsenene[8] and antimonene[13] in the form of the same buckled allotrope. Under a tensile strain of +12% the band gap in indiene changes by 0.92 eV, more than half as much as in arsenene (−1.64 eV), and much closer to the change in antimonene (−0.74 eV), which has a more similar electronic structure. Since buckled indiene preserves its structure under strains of up to 20%, this comparison points out that an efficient band gap modulation can be achieved using in-plane strain, tuning it over a range of almost 1 eV. Using buckled indiene as an optoelectronic nanomaterial is, thus, a promising path to new devices.

An insightful way to describe the changes in the band structure is to study the electronic charge density distribution (Fig. 7). Under no strain, buckled indiene shows a moderately localized distribution of electronic orbitals, which are somewhat distorted along the bonding directions (hexagon sides). The valence state is predominantly localized, whereas the conduction state exhibits a delocalized distribution of electron charge density. Charge densities change critically under mechanical strain. These changes are sufficient to induce a transition in the electronic properties. Specifically, under a negative compressive strain, a large increase in the delocalization of the VBM state along the bonds can be observed. An increased distribution of delocalized electrons decreases the band gap until it closes under a strain of −14%. These electrons become quasi-free and are able to conduct electricity, making the buckled indiene metallic under compressive strain. Under tensile strain the changes are not so significant.

3.3.2 Planar indiene. The effect of strain on the electronic band structure of planar indiene is shown in Fig. 8. Planar indiene keeps its metallic behavior throughout the whole segment of strains used in our calculations. As expected, negative strain closes in the electronic bands, while positive strain spreads them out: valence bands toward more negative and conduction bands toward more positive energies.

The charge distribution of valence electrons is presented in Fig. 9. Aside from the middle hexagon regions, which show no charge density accumulation, the charge is nearly uniformly extended over the two-dimensional indiene plane which contributes to the conductivity. We have also calculated the difference between the charge densities of the system and its atomic constituents. It clearly indicates the presence of covalent bonds, because of the high electronic densities along the bonding directions between the indium atoms.

4 Conclusions

In conclusion, calculations based on a first principles approach show that the planar and buckled structures of a two-dimensional material – indiene, are stable allotropes from both a total energy and lattice dynamics point of view, while the puckered one is dynamically not stable. The total energy of the stable structures (planar and buckled) is nearly equal, meaning that they could both be potentially exfoliated from the bulk indium. The planar allotrope behaves like a metal, with Dirac points in the band structure and a van Hove singularity in the density of states, which could practically lead to an increase in the electronic conductance. On the other hand, the buckled allotrope behaves like an indirect semiconductor with a band gap of almost 1 eV. Using strain engineering, this band gap can be further increased (tensile strain) or even closed (compressive strain) so that it behaves like a metal. Based on the energy band gaps in the proposed two-dimensional systems, we can predict that planar and buckled forms of indiene form good candidates for optoelectronic or nanoelectronic devices, such as memory devices, light emitting diodes and solar cells, which require further experimental verifications.

Acknowledgements

Part of the work has been done using High performance computing facility at K2, IUAC, New Delhi, India.

References

1 K. S. Novoselov, A. K. Geim, S. V. Morozov, D. Jiang, Y. Zhang, S. V. Dubonos, I. V. Grigorieva and A. A. Firsov, *Nature*, 2004, **306**, 666–669.
2 A. K. Geim and K. S. Novoselov, *Nat. Mater.*, 2007, **6**, 183–191.
3 A. H. C. Neto, F. Guinea, N. M. R. Peres, K. S. Novoselov and A. K. Geim, *Rev. Mod. Phys.*, 2009, **81**, 109–162.
4 J. Qiao, X. Kong Kong, Z. X. Hu, F. Yang and W. Ji, *Nat. Commun.*, 2014, **5**, 4475–4481.
5 G. Wang, R. Pandey and S. P. Karna, *Nanoscale*, 2015, **7**, 524–531.
6 P. Bharadwaj and L. Novotny, *Opt. Photonics News*, 2015, 26–31.
7 S. Zhang, Z. Yan, Y. Li, Z. Chen and H. Zeng, *Angew. Chem., Int. Ed.*, 2015, **54**, 3112–3115.
8 C. Kamal and M. Ezawa, *Phys. Rev. B: Condens. Matter Mater. Phys.*, 2015, **91**, 085423–085432.
9 Z. Zhu, J. Guan and D. Tomanek, *Phys. Rev. B: Condens. Matter Mater. Phys.*, 2015, **91**, 161404–161408.
10 Y. Wang and Y. Ding, *J. Phys.: Condens. Matter*, 2015, **27**, 225304–225313.
11 Z. Zhang, J. Xie, D. Yang, Y. Wang, M. Si and D. Xu, *Appl. Phys. Express*, 2015, **8**, 055201–055204.
12 K. Liangzhi, Y. Ma, X. Tan, T. Frauenheim, A. Du and S. Smith, *J. Phys. Chem. C*, 2015, **119**, 6918–6922.
13 G. Wang, R. Pandey and S. P. Karna, *ACS Appl. Mater. Interfaces*, 2015, **7**, 11490–11496.
14 C. Wang, Q. Xia, Y. Nie and G. Guo, *J. Appl. Phys.*, 2015, **117**, 124302–124311.
15 L. Li, Y. Yu, G. J. Ye, Q. Ge, X. Ou, H. Wu, D. Feng, X. H. Chen and Y. Zhang, *Nat. Nanotechnol.*, 2014, **9**, 372–377.
16 H. Liu, A. T. Neal, Z. Zhu, X. Xu, D. Tomanek and P. D. Ye, *ACS Nano*, 2014, **8**, 4033–4041.
17 C. C. Liu, H. Jiang and Y. Yao, *Phys. Rev. B: Condens. Matter Mater. Phys.*, 2011, **84**, 195430.
18 B. Cai, S. Zhang, Z. Hu, Y. Hu, Y. Zou and H. Zeng, *Phys. Chem. Chem. Phys.*, 2015, **17**, 12634–12638.
19 P. Vogt, P. D. Padova, C. Quaresima, J. Avila, E. Frantzeskakis, M. C. Asensio, A. Resta, B. Ealet and G. L. Lay, *Phys. Rev. Lett.*, 2012, **108**, 155501.
20 C.-L. Lin, R. Arafune, K. Kawahara, N. Tsukahara, E. Minamitani, Y. Kim, N. Takagi and M. Kawai, *Appl. Phys. Express*, 2012, **5**, 045802–045804.
21 A. Fleurence, R. Friedlein, T. Ozaki, H. Kawai, Y. Wang and Y. Yamada-Takamura, *Phys. Rev. Lett.*, 2012, **108**, 245501.
22 N. D. Drummond, V. Zólyomi and V. I. Fal'ko, *Phys. Rev. B: Condens. Matter Mater. Phys.*, 2012, **85**, 075423–075429.
23 Z. Ni, H. Zhon, X. Jiang, R. Quhe, G. Luo, Y. Wang, M. Ye, J. Yang, J. Shi and J. Lu, *Nanoscale*, 2014, **6**, 7609–7618.
24 C. Kamal, A. Chakrabarti, M. Ezawa, Aluminene as Highly Hole Doped Graphene, arXiv preprint arXiv:1502.05874.
25 Q. Wei and X. Peng, *Appl. Phys. Lett.*, 2014, **104**, 251915–251919.
26 G. Wang, M. Si, A. Kumar and R. Pandey, *Appl. Phys. Lett.*, 2014, **104**, 213107–213110.
27 K. S. Kim, Y. Zhao, H. Jang, S. Y. Lee, J. M. Kim, K. S. Kim, J.-H. Ahn, P. Kim, J.-Y. Choi and B. H. Hong, *Nature*, 2009, **457**, 706–710.
28 P. Hohenberg and W. Kohn, *Phys. Rev.*, 1964, **136**, B864–B871.
29 W. Kohn and L. J. Sham, *Phys. Rev.*, 1965, **140**, A1133–A1138.
30 P. Giannozzi, P. Giannozziand, S. Baroni, N. Bonini, M. Calandra, R. Car, C. Cavazzoni, D. Ceresoli, G. L. Chiarotti, M. Cococcioni, I. Dabo, A. D. Corso, S. Fabris, G. Fratesi, S. de Gironcoli, R. Gebauer, U. Gerstmann, C. Gougoussis, A. Kokalj, M. Lazzeri, L. Martin-Samos, N. Marzari, F. Mauri, R. Mazzarello, S. Paolini, A. Pasquarello, L. Paulatto, C. Sbraccia, S. Scandolo, G. Sclauzero, A. P. Seitsonen, A. Smogunov, P. Umari and R. M. Wentzcovitch, *J. Phys.: Condens. Matter*, 2009, **21**, 395502–395520.
31 J. P. Perdew, K. Burke and M. Ernzerhof, *Phys. Rev. Lett.*, 1996, **77**, 3865–3868.
32 A. Kokalj, *Comput. Mater. Sci.*, 2003, **28**, 155–168.
33 F. Mazzola, J. W. Wells, R. Yakimova, S. Ulstrup, J. A. Miwa, R. Balog, M. Bianchi, M. Leandersson, J. Adell, P. Hofmann and T. Balasubramanian, *Phys. Rev. Lett.*, 2013, **111**, 216806–216810.
34 G.-Z. Kang, D.-S. Zhang and J. Li, *Phys. Rev. B: Condens. Matter Mater. Phys.*, 2013, **88**, 045113.
35 A. Castellanos-Gomez, *et al.*, *2D Mater.*, 2014, **1**, 025001–025019.
36 L. Li, Y. Yu, G. J. Ye, Q. G. X. O. H. Wu, D. Feng, X. H. Chen and Y. Zhang, *Nat. Nanotechnol.*, 2014, **9**, 372–377.
37 F. Xia, H. Wang and Y. Jia, *Nat. Commun.*, 2014, **5**, 4458.
38 A. Hashimoto, K. Suenaga, A. Gloter, K. Urita and S. Iijima, *Nature*, 2004, **430**, 870–873.
39 Z. Zhu and D. Tománek, *Phys. Rev. Lett.*, 2014, **112**, 176802.
40 C. Dekker, *Phys. Today*, 1999, 22–28.
41 A. S. Rodin, A. Carvalho and A. C. Neto, *Phys. Rev. Lett.*, 2014, **112**, 176801–176805.
42 H. J. Conley, B. Wang, J. I. Ziegler, J. R. F. Haglund, S. T. Pantelide and K. I. Bolotin, *Nano Lett.*, 2013, **13**, 3626–3630.
43 C. Lee, X. Wei, J. W. Kysar and J. Hone, *Science*, 2008, **321**, 385.
44 F. Li, K. Tu, H. Zhang and Z. Chen, *Phys. Chem. Chem. Phys.*, 2015, **17**, 24151–24156.